Radiation of internal waves from groups of surface gravity waves

By S. Haney[1] and W.R. Young[1]

[1]Scripps Institution of Oceanography,
UC San Diego, La Jolla, CA 90237, USA

(Received January 30, 2017)

Groups of surface gravity waves induce horizontally varying Stokes drift that drives convergence of water ahead of the group and divergence behind. The mass flux divergence associated with spatially variable Stokes drift pumps water downwards in front of the group, and upwards in the rear. This "Stokes pumping" creates a deep, Eulerian return flow that wiggles the isopycnals below the wave group, and generates a trailing wake of internal gravity waves. We compute the energy flux from surface to internal waves by finding solutions of the wave-averaged Boussinesq equations in two ($2D$) and three dimensions ($3D$) forced by Stokes pumping at the surface. The $2D$ case is distinct from the $3D$ case in that the stratification must be very strong, or the surface waves very slow for any internal wave radiation at all. On the other hand, in $3D$, internal wave radiation always occurs, just with a larger energy flux as the stratification and surface wave amplitude increase, or as the surface waves slow down. The energy flux from surface waves to internal waves varies as the fourth power of the wave amplitude and of the buoyancy frequency, and is inversely proportional to the fifth power of the surface wave period. Using parameters typical of short period swell (e.g., 8 second surface wave period) we find that the energy flux is small compared to the total energy in a typical surface wave group; therefore this coupling to the internal wave field is not a significant sink of energy for the surface waves. On the other hand, the energy flux may be large enough to be a significant source of energy for internal waves with a spectral peak near the buoyancy frequency.

1. Introduction

Surface gravity waves induce a horizontal Lagrangian mass flux known as the Stokes drift. The Stokes drift is proportional to the square of the amplitude of the waves and thus a slowly varying wave group has a spatially variable horizontal mass transport. The Stokes drift vanishes, as the waves do, at the edges of the group, thereby inducing a horizontal divergence of the vertically integrated Lagrangian transport. The converging Lagrangian mass flux at the front of the group drives water downward, while divergent Lagrangian mass flux at the rear of the group lifts it up. This "Stokes pumping" drives a deep Eulerian return flow, first shown by Longuet-Higgins & Stewart (1964), discussed further by McIntyre (1981) and van den Bremer & Taylor (2015), and depicted in figure 1(a).

The deep return flow beneath a surface wave group in an unstratified fluid is shown in figure 1(a). The positive momentum contained in the vertically integrated Stokes drift is balanced by the momentum in the deep Eulerian return flow so that the total momentum in a large volume is zero (McIntyre 1981). The structure of the deep return flow can

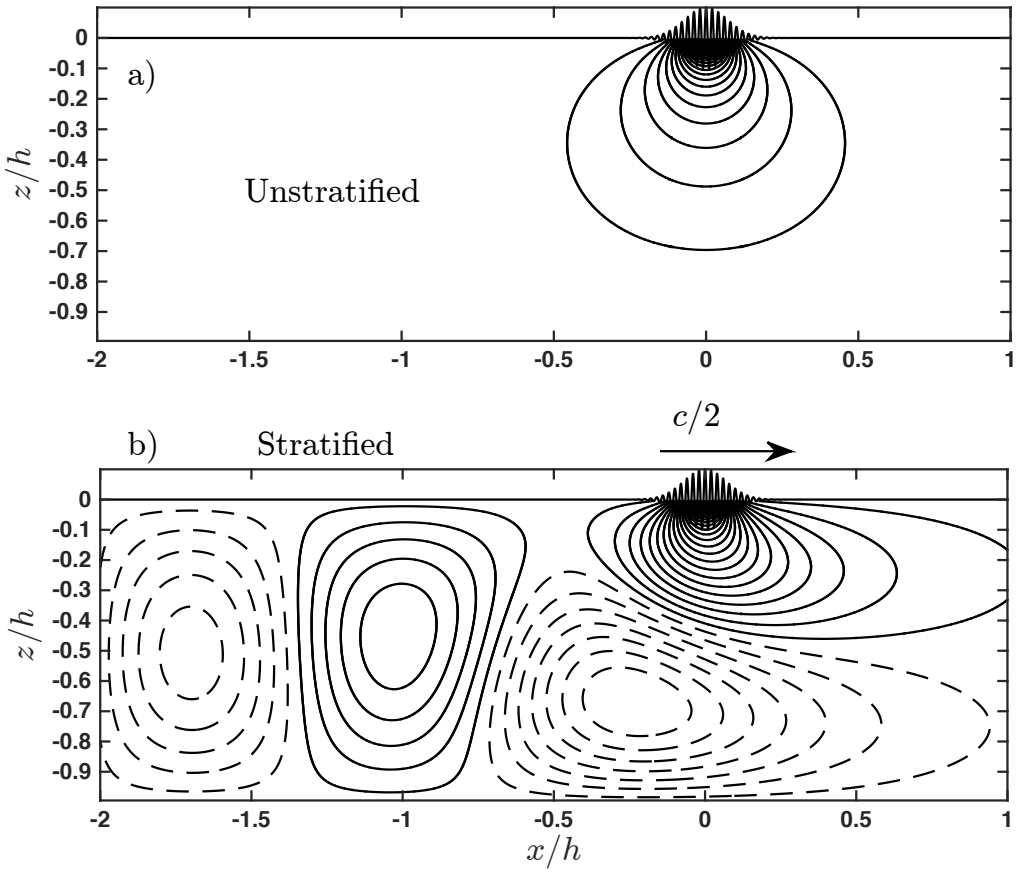

FIGURE 1. (a) The stream function of the deep return flow beneath the gaussian wave group in (A 1) with an unstratified interior. (b) Constant $N = 7 \times 10^{-3} s^{-1}$. The dashed contours indicate negative values of the stream function, and the contour interval is $0.05 m^2 s^{-1}$. In both panels, the surface wave group is moving to the right with group speed $c/2$ with $c = \sqrt{g/k}$. The surface wave amplitude is exaggerated by orders of magnitude in order to visualize the group; in this illustration of a "two-dimensional" group $\ell_x/h = 0.07$ and $\ell_y = \infty$ where ℓ_x and ℓ_y are the horizontal length scales of the gaussian packet in (A 1).

be understood with an electrostatic analogy in which the streamlines are lines of force induced by the dipolar Stokes pumping, essentially at the surface $z = 0$. Consequently, in the two-dimensional (2D) case, the velocity of the deep return flow decays slowly with depth, z, as z^{-2} below the group so that the bottom at $z = -h$ has important effects even in very deep water. In the three-dimensional (3D) case, some of the return flow may go around rather than underneath the surface waves. Thus in the 3D case the decay of deep currents is faster, but still algebraic as z^{-3}(van den Bremer & Taylor 2015).

Here we investigate the effects of stratification on the structure of the Eulerian-mean return flow beneath a group of surface waves. As anticipated by McIntyre (1981), stable stratification greatly modifies the form of the return flow by exciting internal gravity waves as the surface wave group passes above: see figure 1(b).

To make a direct comparison with the unstratified return flow in figure 1(a) we have also shown the stream function in figure 1(b). However, with typical oceanic stratification, the 2D and 3D situations are strikingly different. In the 2D case, the phase speed of the

internal waves is necessarily in the same direction as that of surface wave propagation: in figure 1(b) the x-phase speed of the internal wave train is equal to the surface wave group velocity, $c/2$ with $c = \sqrt{g/k}$. The group speeds of swell with typical wavelengths of 100 meters or greater exceed 5ms^{-1}. But Chelton *et al.* (1998) show that the internal wave phase speed in the ocean never exceeds 3.2ms^{-1}. Thus the radiation of internal waves by strictly 2D surface waves — the situation shown in figure 1(b) — does not occur in Earth's ocean. In other words, ocean stratification is so weak that in the 2D case internal waves cannot keep up with swell and there is no radiation. But in the 3D case in which the surface wave packet has finite extent in the spanwise (y) direction radiated internal waves can propagate obliquely to the direction of propagation (the x-axis) of the surface wave group. With oblique propagation the phase speed of internal waves *along the x-axis* can equal $c/2$ even in a weakly stratified ocean. Thus internal wave radiation from surface wave groups is much more efficient in 3D than in 2D.

The coupling of surface waves and internal waves has been explored previously in oceanography as a possible mechanism for energizing the ocean internal wave field. The recent paper by Olbers & Eden (2016) reviews this oceanographic literature, starting with the first estimates of the strength of surface-wave driving of internal waves (Watson, West & Cohen 1976; Olbers & Herterich 1979). These estimates are based on resonant triad theory and employ a spectral characterization of the surface wave field. Consequently they do not directly indicate the effect of stratification on the situation in Figure 1(b) in which the deep return flow associated with a narrow-band group of ocean swell shakes the deep, stable stratification of the ocean.

However there is a connection between internal wave radiation from the surface wave group in Figure 1(b) and resonant triad theory: radiation of internal waves requires that the phase speed of the internal wave must match the speed of the forcing, which is the group speed of the surface waves. This condition is a special case of triad resonance in which the surface wave group constitutes two members of the triad with close wavenumbers k and $k + \delta k$, and the radiated internal wave is the third member of the triad with wavenumber δk. In this paper we are isolating this particular triad interaction as it applies directly to situation in Figure 1(b) and showing the connection to Stokes drift and the associated deep return flow.

In section 2 we recall the first order in wave amplitude solution in terms of the standard velocity potential; considering the second order in wave amplitude, we perform a phase average to obtain the internal wave equation forced by the divergence of the mean wave momentum at the surface. In section 3 we solve the surface forced internal wave equation to obtain the wave-averaged vertical velocity and pressure. In section 4 we obtain an expression for the energy flux from surface waves to internal waves; in section 5 we discuss the $2D$ limit of the $3D$ energy flux solution. Section 6 is the discussion and conclusion.

2. Formulation

We decompose the density as

$$\rho = \rho_0 \left(1 + \int_z^0 N^2(z')\mathrm{d}z' - g^{-1}b \right) , \tag{2.1}$$

where g is the gravitational acceleration acting in the negative z-direction, $N^2(z)$ is the buoyancy frequency and $b(x, y, z, t)$ is the buoyancy (e.g., Phillips 1977). The Boussinesq

equations are

$$\boldsymbol{u}_t + \boldsymbol{u}\cdot\boldsymbol{\nabla}\boldsymbol{u} + \boldsymbol{\nabla}p = b\hat{\boldsymbol{z}}\,, \tag{2.2}$$

$$b_t + \boldsymbol{u}\cdot\boldsymbol{\nabla}b + wN^2 = 0\,, \tag{2.3}$$

$$\boldsymbol{\nabla}\cdot\boldsymbol{u} = 0\,, \tag{2.4}$$

where the velocity is $\boldsymbol{u} = u\hat{\boldsymbol{x}} + v\hat{\boldsymbol{y}} + w\hat{\boldsymbol{z}}$

We denote the magnitude of the free-surface displacement by $a_{\max}$, the wavenumber of the primary surface wave by k and the horizontal length scale of the surface-wave group in the x-direction by ℓ_x. Using these scales the wave steepness and scale separation parameters are

$$\epsilon \stackrel{\text{def}}{=} a_{\max}k\,, \qquad \text{and} \qquad \mu \stackrel{\text{def}}{=} \frac{1}{k\ell_x}\,. \tag{2.5}$$

We assume that ϵ and μ are both small and we neglect the direct effects of stratification in the shallow wave zone where kz is order one. This assumption is justified provided that the wave frequency $\sqrt{gk}$ is much greater than $N(z)$ in this region. In the along-crest (y) direction, the surface wave group has length ℓ_y; we treat ℓ_y/ℓ_x as order one.

Denoting the free-surface displacement by $\zeta(x,y,t)$, the surface boundary conditions, correct to second order in wave steepness ϵ, are

$$@z = 0: \qquad \zeta_t + (u\zeta)_x + (v\zeta)_y = w\,, \tag{2.6}$$

and

$$@z = 0: \qquad p + \zeta p_z = g\zeta + N^2\tfrac{1}{2}\zeta^2\,. \tag{2.7}$$

In (2.6) and (2.7) we have transferred the surface boundary conditions from the moving free surface $z = \zeta$ to the flat surface $z = 0$ using the Stokes expansion. The bottom boundary condition is $w(x,y,-h,t) = 0$. We confine attention to deep-water waves, $kh \gg 1$, so that the bottom boundary condition is important only for the deep return flow beneath the surface wave group.

Scaling time with the wave frequency $\sqrt{gk}$ and length with the wavenumber k sets $g \to 1$. One then expands all variables in powers of wave steepness ϵ; for example

$$p = \epsilon p_1 + \epsilon^2 p_2 + \cdots \tag{2.8}$$

While we are guided by this scheme, for clarity we develop the expansion using the original dimensional variables.

2.1. *The solution at first order*

In the first-order equations we neglect the small buoyancy force $b_1\hat{\boldsymbol{z}}$ on the right of the momentum equation (2.2). With this approximation the classic first-order solution is irrotational and is expressed using the familiar velocity potential $\phi(x,y,z,t)$:

$$\boldsymbol{u}_1 = \boldsymbol{\nabla}\phi\,, \qquad \text{and} \qquad p_1 = -\phi_t\,. \tag{2.9}$$

The problem then reduces to the solution of the 3D Laplace equation $\phi_{xx}+\phi_{yy}+\phi_{zz} = 0$ with the surface boundary condition $\phi_{tt} + g\phi_z = 0$ at $z = 0$ and the deep-water condition that $\phi(x,y,-\infty,t) = 0$. Correct to leading order in the scale-separation parameter μ, the first-order solution for a surface wave group is

$$\zeta_1 = \tfrac{1}{2}a(\tilde{x},y,0)\exp\left[\mathrm{i}k\,(x-ct)\right] + c.c. \tag{2.10}$$

$$\phi = -\tfrac{1}{2}\mathrm{i}c\,a(\tilde{x},y,z)\exp\left[\mathrm{i}k\,(x-ct) + kz\right] + c.c.\,, \tag{2.11}$$

where $a(\tilde{x}, y, z)$ is the slowly varying envelope, $c = \sqrt{g/k}$ is the surface-wave phase speed, and

$$\tilde{x} \stackrel{\text{def}}{=} x - \tfrac{1}{2}ct\,, \tag{2.12}$$

is the wave-group coordinate; $c/2$ in (2.12) is the deep-water group velocity. We assume that the surface wave phase velocity is parallel to the group velocity. Following van den Bremer & Taylor (2015) we neglect dispersive spreading of the group.

2.2. *Quadratic properties of the first-order solution*

At next order we need several quadratic properties of the first-order solution, some of which are expressed most easily using the first-order wave displacement $\boldsymbol{\xi}_1$ defined via

$$\boldsymbol{\xi}_{1t} = \boldsymbol{u}_1 = \boldsymbol{\nabla}\phi\,. \tag{2.13}$$

At $z = 0$ the vertical displacement $\zeta_1(x, y, z, t) = \hat{\boldsymbol{z}} \boldsymbol{\cdot} \boldsymbol{\xi}_1$ is the same as the first-order displacement of the free surface denoted peviously by $\zeta_1(x, y, t)$; the dynamically negligible buoyancy perturbation in the wave zone is diagnosed as $b_1 = -N^2\zeta_1$.

Denoting a running phase average over the fast oscillation of the primary wave by an overbar, the Stokes drift in the x-direction is

$$u^{\mathrm{S}} \stackrel{\text{def}}{=} \overline{\boldsymbol{\xi}_1 \boldsymbol{\cdot} \boldsymbol{\nabla} u_1} = c\,k^2|a|^2\mathrm{e}^{2kz}\,. \tag{2.14}$$

The mean wave momentum per unit area in the x-direction is $\rho_0 M$, where

$$M \stackrel{\text{def}}{=} \overline{u_1\zeta_1}\big|_0 = \tfrac{1}{2}ck\,|a|^2\,, \tag{2.15}$$

with $\big|_0$ indicating evaluation at $z = 0$. The identity

$$M = \int_{-\infty}^{0} u^{\mathrm{S}}\,\mathrm{d}z \tag{2.16}$$

shows that u^{S} can be interpreted as the vertical distribution of the mean wave momentum (e.g., Phillips 1977). The chain of identities

$$\overline{\zeta_1 p_{1z}} = -\overline{\zeta_1 w_{1t}} = \overline{w_1^2} = \tfrac{1}{2}\overline{|\boldsymbol{u}_1|^2} = \tfrac{1}{2}cu^{\mathrm{S}} \tag{2.17}$$

is useful at next order. The identities in (2.17) express all important wave-averaged quantities in terms of the Stokes drift in (2.14).

2.3. *The second-order wave-averaged equations of motion*

To write the phase-averaged second-order equations compactly we introduce the Bernoulli function

$$\varpi \stackrel{\text{def}}{=} \bar{p}_2 + \tfrac{1}{2}\overline{|\boldsymbol{u}_1|^2}\,, \tag{2.18}$$

which we refer to hereafter, simply as the pressure. Using ϖ, the phase-averaged second-order equations are

$$\bar{\boldsymbol{u}}_{2t} + \boldsymbol{\nabla}\varpi = \bar{b}_2\hat{\boldsymbol{z}}\,, \tag{2.19}$$

$$\bar{b}_{2t} + \overline{w}_2 N^2 = 0\,, \tag{2.20}$$

$$\boldsymbol{\nabla}\boldsymbol{\cdot}\bar{\boldsymbol{u}}_2 = 0\,. \tag{2.21}$$

Although the buoyancy force $b\hat{\boldsymbol{z}}$ has a negligible effect on the surface wave group it does affect the deep flow and therefore it is essential to retain $\bar{b}_2\hat{\boldsymbol{z}}$ in (2.19). Because of the buoyancy force, the deep flow beneath the surface wave group is not irrotational and thus it is not possible to use a velocity potential to represent the solution of (2.19) through

(2.21). Instead the system can be combined to obtain the internal wave equation for the second-order wave-averaged vertical velocity

$$\left[\partial_t^2\left(\partial_x^2+\partial_y^2+\partial_z^2\right)+N^2\left(\partial_x^2+\partial_y^2\right)\right]\bar{w}_2=0\,. \tag{2.22}$$

Combining (2.20) with the vertical part of (2.19), the pressure ϖ can be expressed in terms of the second-order vertical velocity as

$$\varpi_{zt}=-(\partial_t^2+N^2)\bar{w}_2\,. \tag{2.23}$$

The wave-averaged second-order surface boundary conditions following from (2.6) and (2.7) are

$$@z=0: \qquad \bar{\zeta}_{2t}+M_x=\overline{w}_2\,, \tag{2.24}$$

and

$$@z=0: \qquad \varpi=g\bar{\zeta}_2+N^2\tfrac{1}{2}\overline{\zeta_1^2}\,. \tag{2.25}$$

Identity (2.17) has been used to express the surface boundary condition (2.25) in terms of the Bernoulli function ϖ. Following earlier authors (e.g. Longuet-Higgins & Stewart 1964; van den Bremer & Taylor 2015), we make the "rigid-lid approximation" by neglecting $\bar{\zeta}_{2t}$ in the (2.24) so that the surface boundary condition simplifies to

$$@z=0: \qquad \bar{w}_2\approx M_x\,. \tag{2.26}$$

If required, the mean displacement can be diagnosed from (2.25) as $\bar{\zeta}_2\approx g^{-1}\varpi|_0$. The bottom boundary condition is $\bar{w}_2=0$. *A posteriori* scale analysis indicates that the rigid-lid approximation is justified provided that $h/4k\ell_x^2\ll 1$ where ℓ_x is the typical length of the surface wave packet.

3. Radiating solutions of the second-order wave-averaged equations

Solving the internal wave equation (2.22) for the vertical velocity, we encounter a well-known issue in radiation problems: there are zero-denominators related to the resonance condition that the internal wave phase speed in the x-direction must be equal to the surface wave group speed $c/2$. To make sense of this singularity we follow the method of Lighthill (1967, 1978) and assume that the surface wave group has been growing very slowly from $t=-\infty$ at a rate δ. The quasi-steady solution, with the correct radiation condition, is found by taking the limit $\delta\to 0$ through positive values. Thus the boundary condition (2.26) is modified to

$$@z=0: \qquad \bar{w}_2=e^{\delta t}M_x\,, \tag{3.1}$$

with $\delta>0$.

3.1. *Projection onto vertical modes and Fourier transform*

With uniform N we express the solution of the internal wave equation (2.22) and the pressure equation (2.23) as a sum of orthonormal vertical modes:

$$\bar{w}_2=\sum_{n=1}^{\infty}w_n(x,y,t)\,\sqrt{2}\sin m_n z\,, \qquad \text{and} \qquad \varpi=\sum_{n=1}^{\infty}\varpi_n(x,y,t)\,\sqrt{2}\cos m_n z\,, \tag{3.2}$$

where the vertical wavenumber is

$$m_n\stackrel{\text{def}}{=}n\pi/h\,. \tag{3.3}$$

The modal amplitudes in (3.2) are given by

$$(w_n, \varpi_n) = \frac{1}{h}\int_{-h}^{0} (w, \varpi)\,\sqrt{2}\,(\sin m_n z, \cos m_n z)\;\mathrm{d}z\,. \tag{3.4}$$

Projecting the internal wave equation (2.22) onto the sine modes we obtain

$$\left[\partial_t^2\left(\partial_x^2+\partial_y^2-m_n^2\right)+N^2\left(\partial_x^2+\partial_y^2\right)\right] w_n = \frac{\sqrt{2}m_n}{h}\partial_t^2\partial_x e^{\delta t} M\,. \tag{3.5}$$

The forcing on the right hand side of (3.5) comes from handling the z-derivatives in (2.22) with integration by parts.

Moving along with the surface waves we look for a solution of (3.5) of the form $\mathrm{e}^{\delta t} w_n(\tilde{x}, y)$ where $\tilde{x}$ is the group coordinate defined in (2.12). Using the Fourier transform

$$\hat{w}_n(q,s) \stackrel{\text{def}}{=} \iint \mathrm{e}^{-\mathrm{i}(q\tilde{x}+sy)} w_n(\tilde{x}, y)\,\mathrm{d}x\mathrm{d}y\,, \tag{3.6}$$

the solution of (3.5) is

$$\hat{w}_n = -\frac{\sqrt{2}m_n}{h}\,\frac{\mathrm{i}q\,(q+\mathrm{i}\eta)^2\,\hat{M}(q,s)}{(q+\mathrm{i}\eta)^2\,(q^2+s^2+m_n^2)-q_{\max}^2\,(q^2+s^2)}\,, \tag{3.7}$$

where

$$q_{\max} = 2N/c\,, \qquad \text{and} \qquad \eta \stackrel{\text{def}}{=} 2\delta/c\,. \tag{3.8}$$

Projecting the pressure equation (2.23) onto the sine basis functions, and then Fourier transforming, one finds that the modal amplitudes of the pressure field in (3.2) are

$$\hat{\varpi}_n = \frac{\mathrm{i}c}{2m_n}\,\frac{q_{\max}^2-(q+\mathrm{i}\eta)^2}{(q+\mathrm{i}\eta)}\,\hat{w}_n\,. \tag{3.9}$$

The inverse Fourier transform of (3.7)

$$w_n = \iint_{-\infty}^{\infty} \hat{w}_n e^{\mathrm{i}(q\tilde{x}+sy)}\,\frac{\mathrm{d}q\mathrm{d}s}{(2\pi)^2}\,, \tag{3.10}$$

$$= \iint_{(q,s)>0} \cos(sy)\,\Re[\hat{w}_n e^{\mathrm{i}q\tilde{x}}]\mathrm{d}q\mathrm{d}s\,. \tag{3.11}$$

In passing from (3.10) to (3.11) we have exploited the symmetries $\hat{w}_n(q,s) = \hat{w}_n(q,-s)$ and $\hat{w}_n(q,s) = \hat{w}_n^\star(-q,s)$, where * indicates the complex conjugate, to write the inverse Fourier transform as an integral over the first quarter of the wavenumber plane. Here we have assumed that $\hat{M}$ has these same symmetries.

(All wave groups satisfy the reality condition that $\hat{w}_n(q,s) = \hat{w}_n^\star(-q,-s)$, which reduces the integral (3.10) to a half-plane. But the additional symmetry $\hat{w}_n(q,s) = \hat{w}_n(q,-s)$ assumes that the phase and group speeds are parallel and is therefore not compulsory. For example, Smith & Brulefert (2010) observed wave groups in which the wave crests were not parallel to the long axis of the group. For groups such as these, $\hat{M}$ does not have both symmetries assumed in the previous paragraph.)

The vertical velocity is obtained by numerical integration of (3.11) and for illustration we use the surface wave and stratification parameters given in table 1, and choose $\delta = 3.1\times10^{-5}\mathrm{s}^{-1}$ for our slow growth parameter. The horizontal structure of the first four vertical modes is shown in figure 2. Each mode shows a wake of internal waves trailing behind the surface wave group, which is centered at the origin. Figure 3 shows the full vertical velocity for internal waves radiated from a surface wave group passing over a

TABLE 1. Numerical values characteristic of swell and stratification; $g = 9.81\text{ms}^{-2}$ and $\rho_0 = 1000\text{kg m}^{-3}$. Here we have picked parameters for short period swell to emphasize the effect that wave groups have on the internal wave field. The depth averaged stratification, N, is consistent with the phase speed of the first baroclinic mode for a depth $h = 2000\text{m}$. Figure 5 of Chelton *et al.* (1998) shows that the average phase speed of the first baroclinic mode varies with latitude between about 1.5ms^{-1} to 3ms^{-1}. The surface group length, ℓ_x, is based on the assumption that a group is comprised of n_{SW} consecutive waves that are at least half as high as the tallest in the group. While observations of wave group statistics in the North Sea (Battjes & Van Vledder 1984, figure 3b) and in coastal regions (Elgar *et al.* 1984) show that groups of one or two waves are far more likely, five-wave groups are possible.

Parameter	Value Assumed	Typical Range
wavenumber k	$2\pi/(100\,\text{m})$	$2\pi/(100-400\,\text{m})$
frequency $\sqrt{gk}$	$2\pi/(8\,\text{s})$	$2\pi/(8-16\,\text{s})$
phase speed $c=\sqrt{g/k}$,	$12.5\,\text{ms}^{-1}$	$12.5-25\,\text{ms}^{-1}$
wave amplitude $a_{\max}$	$4\,\text{m}$	$0-5\,\text{m}$
number of waves per group n_{SW}	5	$2-10$
group length $\ell_x=\pi n_{SW}/k$	250 m	$100-2000$ m
group width ℓ_y	$3\ell_x = 750m$	$\ell_x - 10\ell_x$
Depth h	2000 m	$1000-6000$ m
depth averaged buoyancy frequency N	$2\pi/(2000\,\text{s})$	$2\pi/(600-10^4\,\text{s})$
$q_{\max}=2N/c$	$2\pi/(12.5\,\text{km})$	$2\pi/(3.75-125\,\text{km})$
(SW group speed)/(IW phase speed) $m_{1*}=cn\pi/2Nh$	3.125	$(0,\infty)$

uniformly stratified ocean. Figure 3 shows strong Stokes pumping in the forcing region with weaker vertical velocities associated with internal waves trailing behind the forcing region. The solution is dominated by the first vertical mode.

3.2. *The singular curves*

Returning to (3.7), we see the problem of zero divisors if we set $\eta = 0$. With small non-zero η the solution is concentrated in wavenumber space on the "singular curve" where the denominator of (3.7) is close to zero. These curves are shown in the first quadrant of the (q,s)-plane in figure 4 for a few values of stratification, depth, and surface wave group speed. The singular curves are defined by the zeros of the function

$$\gamma(q,s) \stackrel{\text{def}}{=} q - q_{\max}\sqrt{\frac{q^2+s^2}{q^2+s^2+m_n^2}}\,. \tag{3.12}$$

The structure of these curves depends on the crucial non-dimensional parameter

$$m_{n*} \stackrel{\text{def}}{=} \frac{m_n}{q_{\max}} = \frac{cn\pi}{2Nh}\,, \tag{3.13}$$

which is the ratio of the surface wave group speed to the approximate internal wave phase speed given by Chelton *et al.* (1998). Figure 4 shows that the case where $m_{n*} \le 1$ is very different from the case $m_{n*} > 1$. The solution shown in figures 2 and 3 has $m_{n*} > 1$ for all vertical mode numbers n.

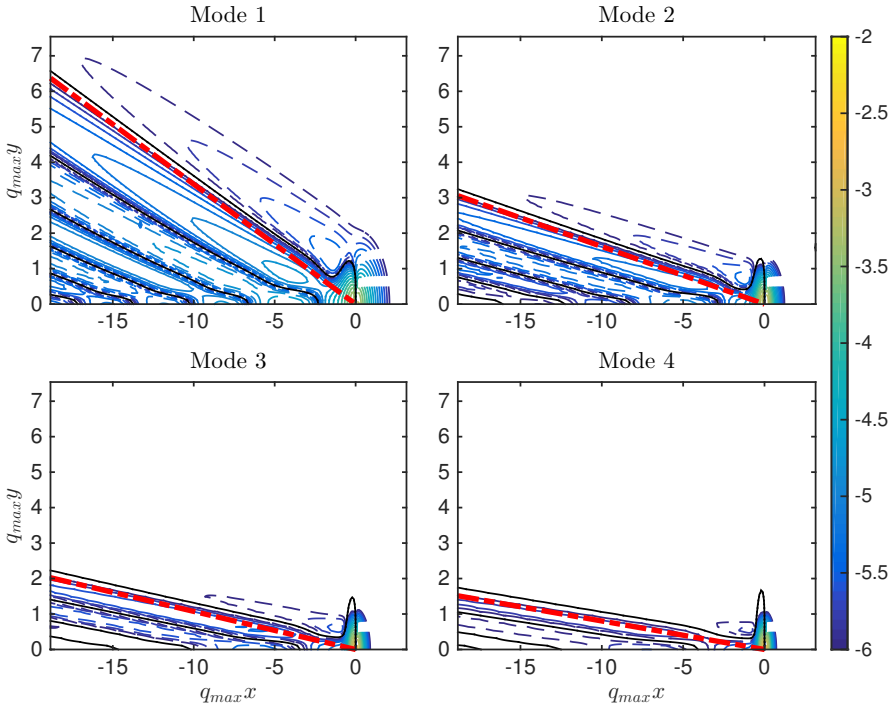

FIGURE 2. Common logarithm of $|w_n|$ for the first four modes. Dashed contours indicate negative vertical velocities. The surface wave group is centered at the origin. The surface wave and stratification parameters are given in table 1. The thin black line is the contour where the vertical velocity vanishes. The red dash-dot line is the theoretical prediction for maximum wake angle given by (3.18).

Using the definition of $q_{\max}$, the condition $\gamma(q,s)=0$ can be re-arranged as

$$\frac{c}{2}=\frac{N}{q}\sqrt{\frac{q^2+s^2}{q^2+s^2+m_n^2}}\,. \tag{3.14}$$

Recalling the internal wave dispersion relation for vertical mode n, namely $\omega^2=N^2(q^2+s^2)/(q^2+s^2+m_n^2)$, we identify the right hand side of (3.14) as the internal wave phase speed in the x-direction. Thus the singular curve (3.14) is the resonance condition that the x-phase speed of the internal waves matches the group velocity $c/2$ of the surface waves. Combining the internal-wave dispersion relation and (3.14) we see that

$$\frac{\omega}{N}=\frac{q}{q_{\max}}\,. \tag{3.15}$$

This relation shows there is an upper bound on the values of q relevant for internal wave radiation: because $\omega<N$, wavenumbers with $q>q_{\max}$ cannot radiate.

3.3. *The wake angle*

The stratification in the ocean is not sufficiently strong to support internal waves that propagate at the surface wave group speed. However, if the radiated internal waves propagate obliquely to the direction of surface wave group propagation then the point of intersection between the internal wave crest and the surface wave group can move with the

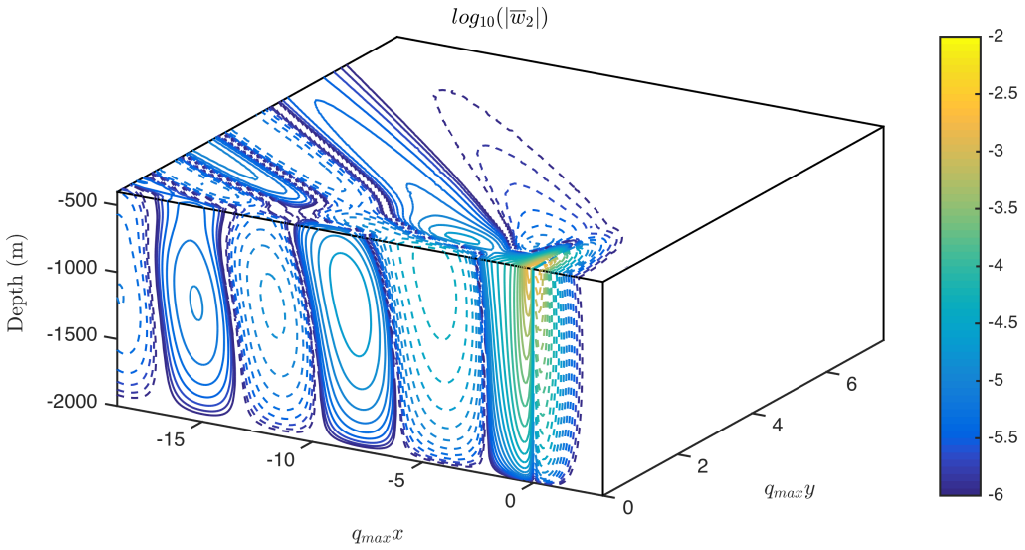

FIGURE 3. Common logarithm of $|\bar{w}_2|$. The surface wave group is centered at the origin, and propagates in the positive x-direction. Dashed contours indicate negative vertical velocities. The surface wave and stratification parameters are given in table 1. The solution shown is a numerical solution of (3.11) with $\delta = 3.1 \times 10^{-5}\text{s}^{-1}$, with 200 vertical modes near the forcing region $[-0.1q_{\max}x : 0.1q_{\max}x]$, and 20 vertical modes in the rest of the domain.

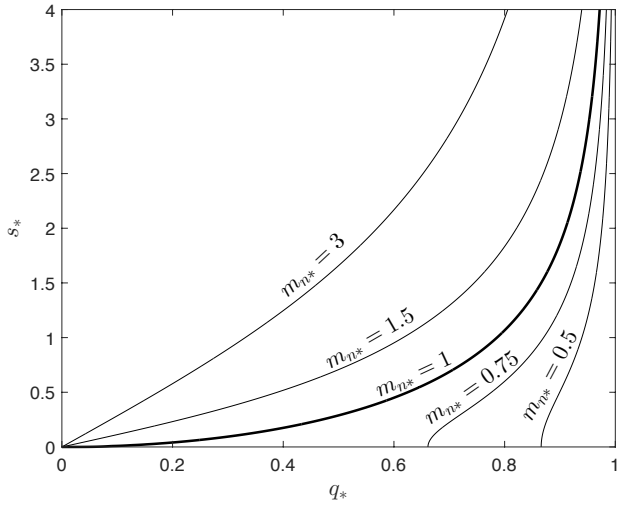

FIGURE 4. The singular curves defined by $\gamma(q, s) = 0$ in the first quadrant of the (q_*, s_*)–plane, where $q_* = q/q_{\max}$, $s_* = s/q_{\max}$, and $m_{n*} = m_n/q_{\max}$. If $m_{n*} \geq 1$ the curve passes through the origin. The curve for $m_{n*} = 1$ is the thick black line.

surface wave group speed. To illustrate this, we will put ourselves in the reference frame moving with the surface wave group. Then the surrounding water is flowing backward at speed $c/2$. As shown in figure 5, this implies that the component of this backward flow that is parallel to the internal wave phase velocity must be equal in magnitude to the internal wave phase velocity. This geometric condition recovers the resonance condition

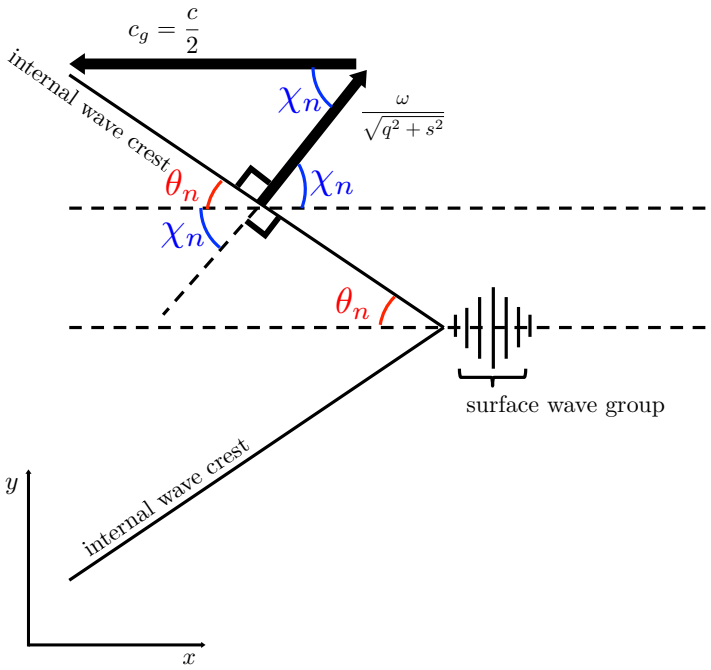

FIGURE 5. Schematic of the internal wave wake in the reference frame where the surface wave group is stationary. The surrounding water rushes backward (to the left) at the group speed $(c/2)$. The internal wave crest intersects the x-axis at and angle θ_n, while the phase velocity of the internal wave, which is perpendicular to its crest, is at an angle of $\chi_n = \pi/2 - \theta_n$ to the x-axis. The condition in (3.16) is that the internal wave crest is stationary because the advance of phase normal to the crest is halted by the normal component, $(c/2)\cos\chi_n$, of the water velocity.

$$\frac{c}{2}\cos\chi_n = \frac{\omega}{\sqrt{q^2+s^2}}\,. \tag{3.16}$$

The wake angle θ_n is related to the direction of the phase velocity, χ_n, by $\theta_n = \pi/2 - \chi_n$, so that $\cos\chi_n = \sin\theta_n$. Therefore the wake angle is

$$\sin\theta_n = \frac{2N}{c\sqrt{q^2+s^2+m_n^2}}\,, \tag{3.17}$$

where we have used the internal wave dispersion relation for $\omega(q,s)$. To find the widest possible wake angle θ_n, we maximize the right hand side of (3.17) over all wavenumbers by taking $q = s = 0$ to find

$$\max_{\forall(q,s)}(\sin\theta_n) = \frac{2N}{cm_n} = \frac{2Nh}{n\pi c} = \frac{1}{m_{n*}}\,. \tag{3.18}$$

The maximum wake angle is determined by the stratification, depth, and surface wave group speed. The first four modal constituents of vertical velocity $w_n(\tilde{x}, y)$ are shown in figure 2. The dashed red line at the angle determined by (3.18) is parallel to the zero contour (the solid, black line), indicating that wake angle predicted by (3.18) is accurate. (Recall in figure 2 that $m_{n*} > 1$ for all n.)

The maximum wake angle in (3.17) is undefined if $m_{n*} < 1$. This is the case if the stratification is strong so the fastest radiated internal waves are moving at the surface wave group speed (e.g., the two-dimensional limit of section 5). Choosing even smaller

values of m_{n*} (larger N, h, or smaller $c/2$) does not change the wake angle beyond $\theta_n = \pi/2$.

4. Energy flux into the internal wave field

The radiation of internal waves from a surface-wave group raises two questions: (1) Is the radiation of internal waves a significant energy sink for the surface waves? and (2) Is this radiation a significant source of energy for the internal waves? In this section we compute the energy flux, and answer these questions with: (1) no and (2) maybe for strong stratification, and slow, large amplitude surface waves.

4.1. *The radiation integral*

From (2.19) through (2.21) we obtain the second-order energy conservation equation

$$\partial_t \tfrac{1}{2}\big(|\boldsymbol{u}_2|^2 + N^{-2}\,\bar{b}_2^2\big) + \boldsymbol{\nabla}\cdot\big(\varpi \boldsymbol{u}_2\big) = 0\,. \tag{4.1}$$

Thus the vertical component of the energy flux at the surface is $\varpi\bar{w}_2\big|_0$; the total flux of energy out of the surface wave group and into the internal wave field in Watts is therefore $\rho_0 J$ where

$$J \stackrel{\text{def}}{=} \iint M_x\,\varpi\big|_0\,\mathrm{d}x\mathrm{d}y\,. \tag{4.2}$$

In (4.2) the surface boundary condition in (2.26) has been used for $\bar{w}_2|_0$. Using the modal expansion for ϖ in (3.2) the right hand side of (4.2) is

$$J = \sum_{n=1}^{\infty} \underbrace{\iint_{-\infty}^{\infty} M_x\,\varpi_n\,\mathrm{d}x\mathrm{d}y}_{\stackrel{\text{def}}{=} J_n}\,, \tag{4.3}$$

where J_n is the energy flux into vertical mode n.

With Parseval's theorem, we can express J_n in terms of the Fourier transforms $\hat{M}$ and $\hat{\varpi}_n$ as

$$J_n = \iint_{-\infty}^{\infty} \mathrm{i}q\hat{M}\hat{\varpi}_n^{\star}\,\frac{\mathrm{d}q\mathrm{d}s}{(2\pi)^2}\,. \tag{4.4}$$

The Fourier transform $\hat{\varpi}_n$ is given by (3.9) and thus the energy flux into vertical mode n is $\rho_0 J_n$ where

$$J_n = \frac{c}{2}\frac{\sqrt{2}}{h}\iint_{-\infty}^{\infty} \frac{\mathrm{i}q^2\left[q_{\max}^2 - (q-\mathrm{i}\eta)^2\right](q+\mathrm{i}\eta)\,|\hat{M}|^2}{(q-\mathrm{i}\eta)^2\,(q^2+s^2+m_n^2) - q_{\max}^2\,(q^2+s^2)}\,\frac{\mathrm{d}q\mathrm{d}s}{(2\pi)^2}\,. \tag{4.5}$$

It is helpful to define

$$\cos^2\vartheta_n = \frac{m_n^2}{q^2+s^2+m_n^2}\,, \qquad \sin^2\vartheta_n = \frac{q^2+s^2}{q^2+s^2+m_n^2}\,, \tag{4.6}$$

so that the partial fraction decomposition of (4.5) can be written as

$$J_n = \frac{c}{2}\frac{\sqrt{2}}{h}\iint_{-\infty}^{\infty} \frac{\mathrm{i}q^2|\hat{M}|^2}{q^2+s^2+m_n^2} \left[q + \mathrm{i}\eta - \tfrac{1}{2}\frac{q_{\max}^2\cos^2\vartheta_n}{q-\mathrm{i}\eta+q_{\max}\sin\vartheta_n} - \tfrac{1}{2}\frac{q_{\max}^2\cos^2\vartheta_n}{q-\mathrm{i}\eta-q_{\max}\sin\vartheta_n}\right]\frac{\mathrm{d}q\mathrm{d}s}{(2\pi)^2}\,. \tag{4.7}$$

We can drop the term $q+\mathrm{i}\eta$ in the square bracket above: the q is an odd function that integrates to zero and the $\mathrm{i}\eta$ is a non-singular term that vanishes in the limit $\eta\to 0$. The remaining terms in the integral are even in both q and s and taking advantage of these symmetries we can restrict the integration to the first quadrant to obtain

$$J_n = -\frac{c}{2}\frac{4\pi q_{\max}^2 m_n^2}{\sqrt{2}h}\iint_{(q,s)>0}\frac{q^2|\hat{M}|^2}{(q^2+s^2+m_n^2)^2}\;\underbrace{\frac{1}{\pi}\frac{\eta}{(q-q_{\max}\sin\vartheta_n)^2+\eta^2}}_{\stackrel{\text{def}}{=}\Delta_\eta(q-q_{\max}\sin\vartheta_n)}\frac{\mathrm{d}q\mathrm{d}s}{(2\pi)^2} \tag{4.8}$$

Taking the limit $\eta\to 0$ in (4.8) using the result in appendix B, we find that the double integral is concentrated on the singular curves given by the zeros of $\gamma(q,s)$ in (3.12), and shown in figure 4. Thus, after the limit $\eta\to 0$ the double integral in (4.8) is reduced to a single integral with respect to q:

$$J_n = -\frac{c}{2}\frac{1}{\sqrt{2}\pi h}\int_{q_{\min}}^{q_{\max}} q^2\left|\hat{M}\big(q,s_n(q)\big)\right|^2\sqrt{\frac{q_{\max}^2-q^2}{m_n^2-q_{\max}^2+q^2}}\,\mathrm{d}q\,. \tag{4.9}$$

In the second argument of $\hat{M}$ in (4.9), the singular curves defined by $\gamma(s,q)=0$, with $\gamma(s,q)$ defined in (3.12), are parameterized by q as $s=s_n(q)$, where

$$s_n(q)\stackrel{\text{def}}{=} q\sqrt{\frac{m_n^2-q_{\max}^2+q^2}{q_{\max}^2-q^2}}\,. \tag{4.10}$$

The upper limit of integration in (4.9) is $q_{\max}=2N/c$ and the lower limit is

$$q_{\min}\stackrel{\text{def}}{=}\begin{cases}0\,, & \text{if } q_{\max}\le m_n;\\ \sqrt{q_{\max}^2-m_n^2}\,, & \text{if } q_{\max}\ge m_n.\end{cases} \tag{4.11}$$

The definition of $q_{\min}$ above corresponds to the distinction between the curves in figure 4 corresponding to $m_{n*}\ge 1$, which pass through the origin, and those curves with $m_{n*}<1$ which cross the q axis at $q=\sqrt{q_{\max}^2-m_n^2}$. Both types of curves asymptote to $s=\infty$ as $q\to q_{\max}$: this asymptote corresponds to the upper limit of integration in (4.9). In physical terms there is a "cut-off" wavenumber $q_{\max}$ because internal waves have frequencies less than N: wavenumbers $q>q_{\max}$ correspond the non-existent internal waves with frequencies greater than N.

The "radiation integral" on the right of (4.9) is our most general expression for the energy lost to mode-n internal gravity waves from the surface wave group. We make approximations to (4.9) assuming realistic surface wave and stratification parameters in section 4.3.

4.2. *Energy transfer between a gaussian surface wave group and the internal wave wake*

To make a simple estimate of the energy loss from surface gravity waves we adopt the gaussian model from appendix A and use numerical values in table 1. Since energy in the surface waves is partitioned equally between kinetic and potential, the total energy of a surface wavetrain is given by $g\zeta_1^2$ (Phillips 1977). Then using ζ_1 in (2.10) and the gaussian wave envelope in (A 1) the energy density of the packet is

$$E=\iint g\zeta_1^2\,\mathrm{d}x\mathrm{d}y=\frac{\pi}{2}ga_{\max}^2\ell_x\ell_y\,. \tag{4.12}$$

Next we non-dimensionalize (4.9) as before using $q_*=q/q_{\max}$ and $m_{n*}=m_n/q_{\max}$,

and replace $|\hat{M}|^2$ gaussian expression (A 3). Using $c^2k = g$, we find

$$J_n = -\frac{q_{\max}^3}{2\sqrt{2}\pi ch}\left(\frac{\pi}{2}ga_{\max}^2\ell_x\ell_y\right)^2 \times \underbrace{\int_{q_{\min *}}^1 q_*^2 \exp\left[-\tfrac{1}{2}(q_{\max}\ell_x)^2 q_*^2\left(1+\frac{m_{n*}^2-1+q_*^2}{1-q_*^2}\,\frac{\ell_y^2}{\ell_x^2}\right)\right]\sqrt{\frac{1-q_*^2}{m_{n*}^2-1+q_*^2}}\,\mathrm{d}q_*}_{\mathcal{J}_n(q_{\max}\ell_x,\ell_y/\ell_x,m_{n*})}, \quad (4.13)$$

where

$$q_{\min *} = \begin{cases} \sqrt{1-m_{n*}^2}\,, & \text{if } m_{n*} < 1; \\ 0\,, & \text{if } m_{n*} \geq 1. \end{cases} \quad (4.14)$$

Using the values in table 1, $q_{\min *} = 0$.

Now we consider the slow time evolution of the surface waves with the internal wave radiation acting as a weak sink of energy:

$$E_t = \sum_{n=1}^{\infty} J_n\,, \quad (4.15)$$

$$= -\underbrace{\frac{q_{\max}^3}{2\sqrt{2}\pi ch}\sum_{n=1}^{\infty}\mathcal{J}_n}_{\stackrel{\text{def}}{=}\alpha}\underbrace{\left(\frac{\pi}{2}ga_{\max}^2\ell_x\ell_y\right)^2}_{E^2}. \quad (4.16)$$

In (4.16) we have expressed the energy flux in terms of the energy in the wave group, and the factor α. We assume that α is constant as $E \propto a_{\max}^2$ slowly decreases due to radiative damping. Then the solution of the differential equation (4.16) is

$$E = \frac{E_0}{1+\alpha E_0 t}\,, \quad (4.17)$$

where E_0 is the initial energy corresponding to the initial $a_{\max}$. Therefore the half-life of a group of surface waves is given by

$$t_{1/2} = \frac{1}{\alpha E_0} = \frac{c^4 h}{\sqrt{2}gN^3 a_{\max}^2\ell_x\ell_y\sum_{n=1}^{\infty}\mathcal{J}_n} = -\frac{E_0}{\sum_{n=1}^{\infty}J_n}\,, \quad (4.18)$$

where $a_{\max}$ and J_n above are evaluated at $t = 0$. Equation (4.18) highlights that faster waves in a deeper ocean survive longer, while larger waves, larger wave groups, and stronger stratification damp the wave group more quickly.

Computing the energy flux from surface to internal waves by numerical evaluation of the integral for J_n in (4.13) we find that the radiated energy into the first 5 vertical modes is approximately 50W. At this rate, it would take over 10,000 days for the surface waves to lose half their energy, in which time the wave group would have traveled more than 100 times around the Earth. We can safely say that this is a small loss of energy from the surface waves.

Might this small energy flux be a significant energy source for the internal wave field? The ocean internal wave spectrum has two peaks: the near-inertial spectral peak and a secondary peak at frequencies close to the buoyancy frequency N (Pinkel 1975). As Olbers & Eden (2016) note, the energy flux from surface waves to internal waves is small compared to the energy flux from the wind into near-inertial waves. However, figure 6 (which is discussed in more detail in section 4.3) shows that the majority of the energy radiated from surface waves goes into near–N internal waves. The amplitude of the near

N spectral peak is roughly 3 orders of magnitude lower than that of the near inertial spectral peak. So the 50W energy flux estimated above may be significant for near–N internal waves. From figure 6 of Pinkel (1975) we estimate this peak in isotherm displacement squared ζ'^2 to be $0.5\mathrm{m}^2(\text{cycle per hour})^{-1}$ in amplitude, and 2 cycles per hour wide. Then we can estimate the near-N internal wave energy density as $\rho N_{pyc}^2 \zeta'^2 h$, where $N_{pyc} = 2\pi/(900\,\mathrm{s})$ is the observed stratification in the pycnocline. Assuming the surface wave and vertically averaged stratification parameters from table 1, the power density of internal wave radiation from surface wave forcing is $\rho_0 \sum_{n=1}^{5} J_n/\ell_x\ell_y$. Then a timescale of forcing, τ, can be obtained by dividing observations of energy density by the power density to find $\tau \approx 2$ days. This implies that roughly two days of forcing the ocean with surface wave groups with these parameters would produce the measured amount of near-N internal wave energy. Keep in mind that in table 1 we have assumed a large value of the surface wave amplitude, $a_{\max} = 4\mathrm{m}$, to highlight this effect. However most of the time the energy flux from surface to internal waves will not be this strong.

4.3. *The limit of weak stratification and fast surface waves*

Figure 2 of Chelton *et al.* (1998), shows a global map of the fastest possible internal wave phase speed based on observations of the vertically integrated stratification, $\int_{-h}^{0} N(z)dz$. This map shows that internal wave phase speeds never exceed $3.2\mathrm{ms}^{-1}$, and generally range from 1 to $3\mathrm{ms}^{-1}$ for the first baroclinic mode. If we consider swell with periods of 8s or larger, then

$$m_{n*} = \frac{cn\pi}{2Nh} \gtrsim 2\,. \tag{4.19}$$

In other words, for surface waves with periods of 8s or longer, the surface wave group speed is always significantly greater than the internal wave phase speed. In this sense the ocean stratification is weak, internal waves are slow, and the surface waves are fast. Thus the relevant case in (4.14) is $m_{n*} > 1$ and $q_{\min *} = 0$. The other case, $m_{n*} < 1$ and $q_{\min *} = \sqrt{1 - m_{n*}^2}$, is not relevant for Earth's oceans.

Equation (4.13) is opaque: the dependence of J_n on key parameters is buried inside a difficult integral. We will exploit the weak stratification and fast surface waves to approximate (4.13), and reveal the dependence of J_n on the stratification and surface wave parameters. After systematic simplification of the integrand in (4.13) assuming $m_{n*}^2 \gg 1$, and $\ell_y > \ell_x$, we have

$$J_n \approx -\frac{1}{n}\frac{\sqrt{2}}{c}\left(Na_{\max}\right)^4 (k\ell_x\ell_y)^2 \underbrace{\int_0^1 q_*^2 \exp\left[-\frac{q_*^2}{1-q_*^2}\frac{(m_n\ell_y)^2}{2}\right]\sqrt{1-q_*^2}\,\mathrm{d}q_*}_{\mathcal{K}_n(m_n\ell_y)}\,. \tag{4.20}$$

Above, $\mathcal{K}_n/m_{n*}$ is an $m_{n*}^2 \gg 1$ approximation to the integral $\mathcal{J}_n$ in (4.13). Using the wave and stratification parameters assumed in table 1, the approximate integrand in (4.20), is very close to the exact integrand in (4.13): see Figure 6. Note that while the exact $\mathcal{J}_n$ in (4.14) depends on three parameters, the approximation $\mathcal{K}_n$ in (4.20) contains only the single parameter $m_n\ell_y$, which is equal to the product of the three parameters in $\mathcal{J}_n$. Therefore

$$J \approx -\frac{\sqrt{2}}{c}\left(Na_{\max}\right)^4 (k\ell_x\ell_y)^2 \sum_{n=1}^{\infty}\frac{1}{n}\mathcal{K}_n(m_n\ell_y)\,, \tag{4.21}$$

provided that $m_{n*} \gg 1$ and ℓ_y/ℓ_x is not too small.

Figure 7 shows the dependence of the integral $\mathcal{K}_n/m_{n*}$ on the control parameter $m_n\ell_y$.

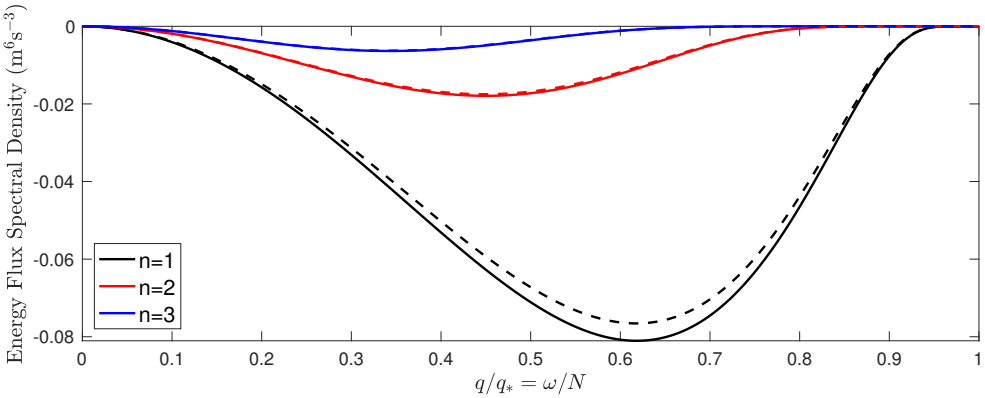

FIGURE 6. The energy flux spectral density for the surface wave and stratification parameters in table 1. The solid lines show the exact integrand in (4.13), and the dashed lines show the approximate in (4.20) for the first three vertical modes as a function of normalized horizontal wavenumber, $q/q_{\max}$, which is equivalent to the internal wave frequency, ω, normalized by the buoyancy frequency, N.

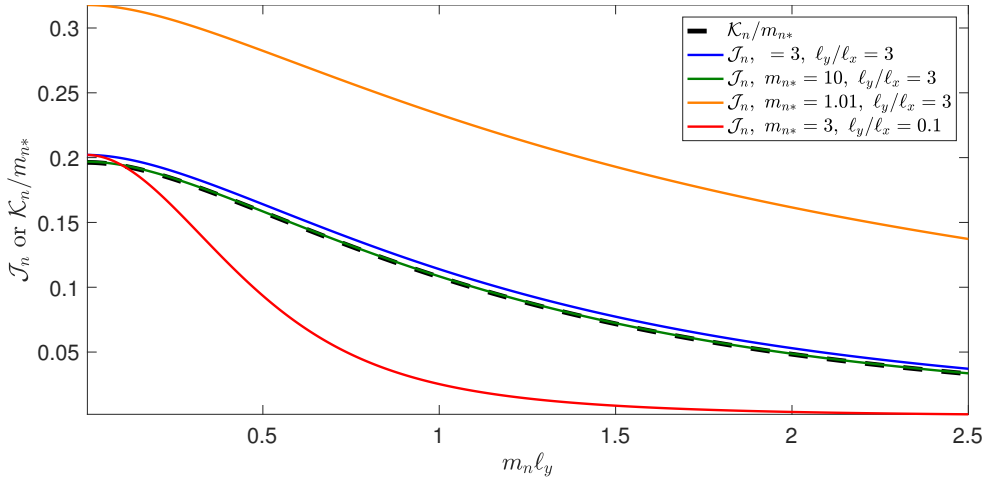

FIGURE 7. The approximate dimensionless integral $\mathcal{K}_n/m_{n*}$ (dashed) compared with exact solutions $\mathcal{J}_n$ (solid) over a range of the control parameter $m_n\ell_y$. The approximation agrees well in two cases where the assumptions ($m_{n*}^2 \gg 1$ and $\ell_y > \ell_x$) are met (blue and green). The approximation is very poor when the assumptions are not met (orange and red)

The dashed line is $\mathcal{K}_n/m_{n*}$, and the solid lines are exact $\mathcal{J}_n$'s from (4.13). The approximation agrees well with the two exact solutions with parameters that satisfy the assumptions $m_{n*}^2 \gg 1$ and $\ell_y > \ell_x$, and very poorly with cases that do not satisfy these inequalities. We see from (4.21) and from figure 7 that the energy flux decreases quickly with increasing n. This is also clear in figure 6. Therefore, neglecting all but the first mode, the energy flux becomes

$$J \approx J_1 \approx -\frac{32\sqrt{2}\pi^5}{g^3}\frac{(Na_{\max})^4}{T^5}(\ell_x\ell_y)^2\,\mathcal{K}_1(m_1\ell_y)\,, \tag{4.22}$$

where we have replaced the wavenumber k and phase speed c with an expression including g and the surface wave period T using the deep water dispersion relation. From (4.22) it is clear that the surface wave amplitude, stratification, and wave period are the strongest

controlling parameters. Thus even small changes in T, $a_{\max}$ and N can drastically change the rate of energy flux from surface to internal waves.

5. The 2D limit for Gaussian wave groups: a special case

The $2D$ problem is significantly simpler than the $3D$ problem discussed in the previous sections. If there is no dependence on y then the streamfunction-vorticity formulation provides a compact solution of the second-order wave-averaged equations of motion. Moreover, Lighthill (1978) in section 3.9, and Lamb (1932) in section 249, provide a resolution of the 2D radiation condition that avoids the technicalities of zero divisors and the $\eta \to 0$ limit in Appendix B. But this resolution does not extend to the 3D problem. For brevity we do not show the details of this specialized 2D calculation. We note that the resulting expression for 2D radiation into vertical mode n is

$$J_n^{2D} = -\frac{cm_n^2}{2h}\left|\hat{M}^{1D}(q_{\min})\right|^2, \tag{5.1}$$

where $\hat{M}^{1D}(q)$ is the 1D (in x) Fourier transform of the wave momentum $M(\tilde{x})$ and

$$q_{\min} = \sqrt{q_{\max}^2 - m_n^2}\,. \tag{5.2}$$

The flux of energy in Joules into the internal wave field is $\rho_0 L_y J_n^{2D}$ where L_y is the length of the system in the y-direction. In the illustrative case of a gaussian envelope in (A 4) and (A 5), the radiation flux in (5.1) is

$$J_n^{2D} = -\frac{m_n^2}{2ch}\left(\frac{\sqrt{\pi}}{2} g a_{\max}^2 \ell_x\right)^2 \mathrm{e}^{-(q_{\min}\ell_x)^2/2}\,. \tag{5.3}$$

In (5.1) and (5.3), and throughout this section, we are assuming that $q_{\max} = 2N/c$ is greater than m_n so that $q_{\min}$ in (5.2) is real. This condition is necessary for the radiation of internal wave energy: with $s = 0$ the resonance condition for vertical mode n is that $c/2$ is equal to $N/\sqrt{q^2 + m_n^2}$, or equivalently that q is equal to $q_{\min}$ in (5.2). The results of Chelton *et al.* (1998) indicate that throughout Earth's ocean the surface wave group speed, $c/2$, for swell is likely greater than the internal wave phase speed N/m_n for all n. In this case $q_{\min}$ in (5.2) is imaginary and there is no radiation.

Nonetheless, as a consistency check on the previous 3D calculations, it is interesting to suppose that $q_{\min}$ is real and show that the 2D results in (5.1) and (5.3) are recovered by taking the limit $\ell_y \to \infty$ in the 3D radiation integral (4.9). The $\ell_y \to \infty$ limit is tricky e.g, as $\ell_y \to \infty$, $\hat{M}(q,s) \propto \delta(s)$ and a straightforward calculation using (4.9) requires consideration of $|\hat{M}|^2 \propto \delta[s_n(q)]^2$. The argument of the squared δ-function, $s_n(q)$, is zero at $q = q_{\min}$. But at this same point the big square root in (4.9) has an integrable singular.

To avoid involvement with these dueling singularities, we first insert $|M|^2$ in (A 3) into (4.9) and then consider $\ell_y \to \infty$:

$$J_n = -\frac{1}{2\pi ch}\left(\frac{\pi}{2} g a_{\max}^2 \ell_x\right)^2 \sqrt{\pi}\ell_y \int_{q_{\min}}^{q_{\max}} q^2 e^{-(q\ell_x)^2/2} \underbrace{\sqrt{\frac{q_{\max}^2 - q^2}{m_n^2 - q_{\max}^2 + q^2}}}_{q/s_n(q)} \underbrace{\lim_{\ell_y\to\infty} \frac{\ell_y}{\sqrt{2}}\frac{1}{\sqrt{\pi}} e^{-(s_n(q)\ell_y)^2/2}}_{\to\delta[s_n(q)]}\,\mathrm{d}q\,. \tag{5.4}$$

The factor ℓ_y left outside the integral in (5.4) is expected on physical grounds: the radiation should be linearly proportional to the length–in–y of the surface wave packet.

Now recall that $s_n(q)$ is defined in (4.10), and observe that $s_n(q_{\min}) = 0$. We can now simplify the integrand in (5.4) using a standard results for δ-functions:

$$\frac{q}{s_n(q)}\,\delta\left[s_n(q)\right] = \frac{q}{s_n(q)}\,\frac{\delta(q-q_{\min})}{\mathrm{d}s_n/\mathrm{d}q}\,, \tag{5.5}$$

$$= \frac{m_n^2}{q_{\min}^2}\,\delta(q-q_{\min})\,. \tag{5.6}$$

Evaluating (5.4) with the δ-function in (5.6) we obtain

$$J_n = \sqrt{\pi}\ell_y J_n^{2D}\,, \tag{5.7}$$

where J_n^{2D} is given by (5.3) and $\sqrt{\pi}\ell_y$ is the effective length in y of the surface wave packet.

6. Discussion

As groups of surface waves pass over the ocean, water is pumped downward in front of the group, and lifted in the rear of the group, inducing a deep return flow. This Stokes pumping is a result of stronger Stokes drift in the center of the group than at the edges, producing a divergence in the mass flux. Without stratification, this produces the deep return flow with momentum equal in magnitude but opposite in direction to the momentum of the shallow Stokes drift. As these wave groups pass over a uniformly stratified ocean, the isopycnals are wiggled by the return flow, generating a trailing wake of internal gravity waves.

Stokes pumping sets the phase of the trailing internal waves, which remain phase locked to the energy source, in this case the surface waves, just as ship wake waves are phase locked to the ship. Since the stratification in the ocean is relatively weak, there are rarely if ever internal waves that propagate with phase speeds as fast as the group speed of swell ($\gtrsim 6\mathrm{ms}^{-1}$). This requires that the internal wave propagate obliquely to the surface wave propagation direction. Then, the internal wave phase speed in the surface wave direction is much faster than the internal wave phase speed in its own propagation direction.

The wake angle can be predicted as a function of the vertical mode number, stratification, surface wave group speed, and ocean depth. The full wake solution shows a wake at nearly the angle appropriate for a mode one wave. This is consistent with the fact that most of the radiated energy is put into mode one internal waves at frequencies near the buoyancy frequency.

Using realistic parameters for surface waves, and ocean stratification, we find that the total energy lost from surface waves is insignificant. However, when the surface waves have very large amplitude and are slow, and when the stratification is strong, the radiation of internal waves may be a significant source for near-N internal waves. Pinkel (1975) observed a near-N spectral peak of internal wave energy. The energy content of this peak divided by the energy flux from surface to internal waves, derived here, gives a timescale of about two days. This implies that this forcing mechanism acting over two days would generate internal waves at near-N frequencies with the observed amount of energy. Therefore, although the very large amplitude swell assumed here is not present everywhere all the time, it suggests that this forcing mechanism may at least contribute to the observed near-N spike in internal wave energy.

Appendix A. A gaussian envelope

For illustrative purposes we use the gaussian envelope function

$$a = a_{\max} \exp\left(-\frac{\tilde{x}^2}{2\ell_x^2} - \frac{y^2}{2\ell_y^2}\right), \tag{A 1}$$

where $\tilde{x}$ is the group coordinate in (2.12). With the envelope in (A 1) the wave momentum (2.15) is

$$M(\tilde{x}, y) = \tfrac{1}{2} c k a_{\max}^2 \exp\left(-\frac{\tilde{x}^2}{\ell_x^2} - \frac{y^2}{\ell_y^2}\right). \tag{A 2}$$

Using the Fourier transform defined in (3.6) we have

$$\hat{M}(q, s) = \tfrac{1}{2} c k a_{\max}^2 \ell_x \ell_y \, \pi \exp\left[-\left(\frac{q\ell_x}{2}\right)^2 - \left(\frac{s\ell_y}{2}\right)^2\right]. \tag{A 3}$$

In the radiation integral for J_n in (4.9) we have $|\hat{M}|^2$.

In section 5 we consider the 2D problem with a gaussian envelope

$$M^{1D}(\tilde{x}) = \tfrac{1}{2} c k a_{\max}^2 \mathrm{e}^{-\tilde{x}^2/\ell_x^2}, \tag{A 4}$$

with Fourier transform

$$\hat{M}^{1D}(q) = \tfrac{1}{2} c k a_{\max}^2 \sqrt{\pi} \ell_x \mathrm{e}^{-(\ell_x q/2)^2}. \tag{A 5}$$

Appendix B. A δ-function limit

The radiation integral in (4.8) has the form

$$I \stackrel{\text{def}}{=} \lim_{\eta \to 0} \iint F(q, s) \underbrace{\frac{1}{\pi} \frac{\eta}{\gamma(q, s)^2 + \eta^2}}_{\Delta_\eta(\gamma)} \, \mathrm{d}q\mathrm{d}s, \tag{B 1}$$

where the function $\gamma(q, s)$ defined in (3.12) is zero on the "singular curve" $\mathcal{C}$. In the limit $\eta \to 0$, the double integral in (B 1) can be reduced to the single integral

$$I = \int_{\mathcal{C}} \frac{F\big(q(\ell), s(\ell)\big)}{\big|\boldsymbol{\nabla}\gamma\big(q(\ell), s(\ell)\big)\big|} \, \mathrm{d}\ell, \tag{B 2}$$

where ℓ is arclength along $\mathcal{C}$. (The result above assumes that in (B 1) $\eta \to 0$ through positive values: the sign is flipped if $\eta \to 0$ through negative values.)

To prove (B 2), note that in terms of intrinsic coordinates (ℓ, n)

$$\mathrm{d}q\mathrm{d}s = \mathrm{d}\ell\mathrm{d}n = \frac{\mathrm{d}\ell\mathrm{d}\gamma}{|\boldsymbol{\nabla}\gamma|}, \tag{B 3}$$

where n is the normal distance from $\mathcal{C}$. Using (B 3) to convert (B 1) to a (γ, ℓ)-integral and

$$\int_{-\infty}^{\infty} \frac{1}{\pi} \frac{\eta}{\gamma^2 + \eta^2} \, \mathrm{d}\gamma = 1, \tag{B 4}$$

to perform the integration over the coordinate γ, we obtain (B 2).

Now suppose that $\mathcal{C}$ is a graph and can therefore be parameterized as $s = f(q)$. The element of arclength is

$$\mathrm{d}\ell = \sqrt{1 + f'^2} \, \mathrm{d}q = \frac{|\boldsymbol{\nabla}\gamma|}{|\gamma_s|} \, \mathrm{d}q. \tag{B 5}$$

Thus, using q to parameterize $\mathcal{C}$, the integral in (B 2) becomes

$$I = \int \frac{F\big(q, f(q)\big)}{\big|\gamma_s\big(q, s(q)\big)\big|}\, \mathrm{d}q\,. \tag{B 6}$$

REFERENCES

Battjes, J. & Van Vledder, G. 1984 Verification of Kimura's theory for wave group statistics. In *Proc., 19th Int. Conf. Coastal Eng*, pp. 642–648.

Chelton, D. B., Deszoeke, R. A., Schlax, M. G., El Naggar, K. & Siwertz, N. 1998 Geographical variability of the first baroclinic rossby radius of deformation. *Journal of Physical Oceanography* **28** (3), 433–460.

Elgar, S., Guza, R. & Seymour, R. 1984 Groups of waves in shallow water. *J. Geophys. Res* **89** (C3), 3623–3634.

Lamb, H. 1932 *Hydrodynamics*. Cambridge University Press.

Lighthill, M. 1967 On waves generated in dispersive systems to travelling forcing effects, with applications to the dynamics of rotating fluids. *Journal of Fluid Mechanics* **27** (4), 725–752.

Lighthill, M. 1978 *Waves in Fluids*. Cambridge University Press.

Longuet-Higgins, M. S. & Stewart, R. 1964 Radiation stresses in water waves; a physical discussion, with applications. *Deep Sea Research* **11** (4), 529–562.

McIntyre, M. 1981 On the 'wave momentum' myth. *Journal of Fluid Mechanics* **106**, 331–347.

Olbers, D. J. & Eden, C. 2016 Revisiting the generation of internal waves by resonant interaction with surface waves. *Journal of Physical Oceanography* **46** (5).

Olbers, D. J. & Herterich, K. 1979 The spectral energy transfer from surface waves to internal waves. *Journal of Fluid Mechanics* **92** (02), 349–379.

Phillips, O. M. 1977 *The Dynamics of the Upper Ocean*. Cambridge University Press.

Pinkel, R. 1975 Upper ocean internal wave observations from flip. *Journal of Geophysical Research* **80** (27), 3892–3910.

Smith, J. A. & Brulefert, C. 2010 Evolution of persistent wave groups. *Journal of Physical Oceanography* **40** (1), 67–84.

van den Bremer, T. & Taylor, P. 2015 Estimates of lagrangian transport by surface gravity wave groups: the effects of finite depth and directionality. *Journal of Geophysical Research Oceans* **120** (4), 2701–2722.

Watson, K. M., West, B. J. & Cohen, B. I. 1976 Coupling of surface and internal gravity waves: a mode coupling model. *Journal of Fluid Mechanics* **77** (01), 185–208.